Key Engineering Materials *Online: 2007-03-15*
ISSN: 1662-9795, Vols. 334-335, pp 613-616
doi:10.4028/www.scientific.net/KEM.334-335.613

Numerical Investigation of Post Buckling Strength and Failure Modes in Advanced Grid Stiffened Structure Under Thermal-Mechanical Loads

Ruixiang Bai[1]， Bo Chen[1]， Cheng Yan[2]， Lin Ye[2]，

Zecheng Li[1] and Haoran Chen[1]

1. State Key Laboratory of Structural Analysis of Industrial Equipment, Department of Engineering Mechanics, Dalian University of Technology, Dalian 116024, Peoples' Republic of China
2. Centre for Advanced Materials Technology, School of Aerospace, Mechanical and Mechatronic Engineering, University of Sydney, NSW 2006, Australia)

[1]Bairx@dlut.edu.cn , [2]ycheng@aeromech.usyd.edu.au

Keywords：Composite; advanced grid stiffened structure; thermal effects; progressive failure

Abstract. This work investigated the post buckling strength and failure behavior of advanced grid stiffened structures (AGS) under thermal-mechanical load using a finite element method. Based on the first order shear deformation theory (FSDT), Von Karman non-linear deformation assumption, and a progressive failure criterion, the buckling, large deformation，local failure modes in the AGS were studied. The thermal effect was also analyzed. By some numerical examples, the failure characteristics of the AGS were discussed.

Introduction

Advanced Grid Stiffened Structures (AGS) have long been of interest as a replacement for honey-comb sandwich and aluminum isogrid constructions due to their particular advantages, such as high impact damage resistance, high damage tolerance, high bending stiffness, high strength and the potential for automated manufacture. Recently, as some new manufacture techniques and innovative tooling concepts have been introduced[1], not only multifarious manufacturing process has been remarkably simplified, but also manufacturing cost has been reduced greatly. As a result, the AGS has a wide application in today's aerospace and aircraft industries such as aircraft fuselage, launch vehicle fuel tanks as well as business jets and manmade satellites[2].

It is well known that delamination, interface debonding, macro-cracks of resin matrix, stiffness degradation and sensitivity to temperature and moisture[3,4] are the common flaws of composite structures, and there is no exception in a AGS. With the powerful numerical analysis methods, more comprehensive understanding of the mechanical properties of AGS, such as load bearing capacity, damage evolution and failure modes can be obtained and this will be essential for design and fabrication of a AGS. In this paper, post buckling strength and failure analysis for the AGS under thermal-mechanical loads has been carried out using FEM method.

Formulation

A typical AGS structure is characterized by a shell structure supported by a lattice pattern of ribs, as shown in Fig.1. In present analysis, the AGS can be simulated by the combination of plate and beam elements. For plate element, the von Karman non-linear relationships between strain and displacement in FSDT are given as follows:

$$\{\boldsymbol{e}\} = \{\boldsymbol{\varepsilon}\} + z\{\boldsymbol{\kappa}\} = \{\boldsymbol{\varepsilon}_m\} + \{\boldsymbol{\varepsilon}_\theta\} + z\{\boldsymbol{\kappa}\}. \tag{1}$$

$$\{\boldsymbol{\gamma}\} = \{\gamma_{yz} \quad \gamma_{xz}\}^T . \tag{2}$$

where

$$\{\boldsymbol{\varepsilon}_m\}=\{u_{,x} \quad v_{,y} \quad u_{,y}+v_{,x}\}^T, \qquad \{\boldsymbol{\varepsilon}_\theta\}=\frac{1}{2}\{w^2{}_{,x} \quad w^2{}_{,y} \quad 2w_{,x}\, w_{,y}\}^T. \tag{3}$$

$$\{\boldsymbol{\kappa}\}=\{\theta_{y,x} \quad -\theta_{x,y} \quad \theta_{y,y}-\theta_{x,x}\}^T, \qquad \{\boldsymbol{\gamma}\}=\{\gamma_{yz} \quad \gamma_{xz}\}^T. \tag{4}$$

Here, u, v, and w are the displacements in the x, y, and z directions, respectively; θ_x and θ_y are rotation in the xz- and yz-planes respectively.

For a laminated plate subjected to a temperature change ΔT, the in-plane thermal load and moment vectors can be obtained by the following formula

$$\{\Delta \boldsymbol{N}_T \quad \Delta \boldsymbol{M}_T\}=\sum_{k=1}^{n}\int_{z_k}^{z_{k-1}}[\overline{\boldsymbol{Q}}]_k\{\overline{\boldsymbol{\alpha}}\}_k(1,z)\Delta T dz\,. \tag{5}$$

The corresponding constitutive relationships can be obtained by integrating the stress-strain equations

$$\begin{Bmatrix}\boldsymbol{N}\\ \boldsymbol{M}\end{Bmatrix}=\begin{bmatrix}\boldsymbol{A} & \boldsymbol{B}\\ \boldsymbol{B} & \boldsymbol{D}\end{bmatrix}\begin{Bmatrix}\boldsymbol{\varepsilon}\\ \boldsymbol{\kappa}\end{Bmatrix}-\begin{Bmatrix}\boldsymbol{\Delta N_T}\\ \boldsymbol{\Delta M_T}\end{Bmatrix}, \qquad \{\boldsymbol{H}\}=\begin{Bmatrix}H_{yz}\\ H_{xz}\end{Bmatrix}=\begin{bmatrix}A_{44} & A_{45}\\ A_{45} & A_{55}\end{bmatrix}\{\boldsymbol{\gamma}\}. \tag{6}$$

where N, M and H are in-plane load, moment and transverse load vectors, respectively.

For beam element, the displacement fields of beam satisfying the compatibility conditions between skin and ribs are assumed as

$$u^b=u+z\theta_y-d\theta_y, \quad v^b=v-z\theta_x, \quad w^b=w. \tag{7}$$

The strain-displacement relationships can be given as follows:

$$\{e^b\}=\{\boldsymbol{\varepsilon}_m\}+\{\boldsymbol{\varepsilon}_n\}=\{u_{,x}+z\theta_{y,x}-d\theta_{y,x} \quad -z\theta_{x,x} \quad w_{,x}+\theta_y\}^T+\{w,^2{}_x/2 \quad 0 \quad 0\}^T. \tag{8}$$

The constitutive equations for a rib considering any temperature change ΔT can be written as follows:

$$\begin{Bmatrix}\sigma_x^b\\ \tau_{xy}^b\end{Bmatrix}=\begin{bmatrix}\overline{Q}_{11} & \overline{Q}_{16}\\ \overline{Q}_{16} & \overline{Q}_{66}\end{bmatrix}\left(\begin{Bmatrix}e_x^b\\ \gamma_{xy}^b\end{Bmatrix}-\begin{Bmatrix}\alpha_x^b\\ \alpha_{xy}^b\end{Bmatrix}\Delta T\right), \qquad \tau_{xz}^b=\overline{Q}_{55}\gamma_{xz}. \tag{9}$$

Progressive damage failure criteria

Three kinds of failure are considered during the postbuckling process, namely matrix failure, fiber failure and fiber-matrix shear failure [5]:

(1) Matrix damage

$$\begin{aligned}&\frac{\sigma_{22}}{Y_c}\left[\left(\frac{Y_c}{2S_{23}}\right)^2-1\right]+\left(\frac{\sigma_{22}}{2S_{23}}\right)^2+\left(\frac{\tau_{12}}{S_{12}}\right)^2+\left(\frac{\tau_{13}}{S_{13}}\right)^2+\left(\frac{\tau_{23}}{S_{23}}\right)^2=1 \quad (\sigma_{22}<0),\\ &\left(\frac{\sigma_{22}}{Y_t}\right)^2+\left(\frac{\tau_{12}}{S_{12}}\right)^2+\left(\frac{\tau_{13}}{S_{13}}\right)^2+\left(\frac{\tau_{23}}{S_{23}}\right)^2=1 \qquad (\sigma_{22}>0).\end{aligned} \tag{10}$$

When Eq.10 is satisfied, $E_2\to 0$, $v_{12}\to 0$.

(2) Fiber fracture

$$\frac{-\sigma_{11}}{X_c}=1 \quad (\sigma_{11}<0), \qquad \frac{\sigma_{11}}{X_c}=1 \quad (\sigma_{11}>0). \tag{11}$$

When Eq.11 is satisfied, $E_1 \to 0$, $E_2 \to 0$, $v_{12} \to 0$, $G_{12} \to 0$, $G_{13} \to 0$, $G_{23} \to 0$.

(3) Fiber-matrix shear damage

$$\left(\frac{\sigma_{11}}{X_c}\right)^2 + \left(\frac{\tau_{12}}{S_{12}}\right)^2 + \left(\frac{\tau_{13}}{S_{13}}\right)^2 = 1 \quad (\sigma_{11} < 0), \qquad \left(\frac{\tau_{12}}{S_{12}}\right)^2 + \left(\frac{\tau_{13}}{S_{13}}\right)^2 = 1 \qquad (\sigma_{11} > 0). \tag{12}$$

When the Eq.12 is satisfied, $v_{12} \to 0$, $G_{12} \to 0$, $G_{13} \to 0$.

Numerical discussions

Considering a grid stiffened cylinder shell (Fig.1), the geometric parameters of the shell are R=100mm and L=500mm. Each ply in the $[50_4/-50_4/50_4/-50_4/50_4]$ laminated skin is 0.125mm thick with material properties of E_{11}=53.8GPa, E_{22}=18.0GPa, G_{12}=8.6GPa, υ=0.25, $X_t = X_c$=1030MPa, Y_T=27.6MPa , Y_C=138.0Mpa, S=41.4MPa, thermal expansion coefficients $\alpha_1 = 6.3\times10^{-6}/°C$, $\alpha_2 = 20.5\times10^{-6}/°C$. The section of the rib is rectangle with a width b=10mm, and height h=6mm. Each ply in the rib is placed along its axial orientation. The separations of circumferential ribs and inclined ribs are 83.33mm and 46.86mm, respectively. The slope angle of the inclined ribs is 0.34rad.The boundary condition is set as one edge clamped, and the other edge is simply supported, but the axial displacement is free.

By Eigenvalue buckling analysis, the critical load of the grid stiffened shell is 13.7 KN/mm and the buckling mode is shown as Fig.2. Compared with post buckling mode obtained by geometric nonliear analysis (Fig.3), the difference is quite apparent because the local buckling behavior occurs at different locations of the shell.

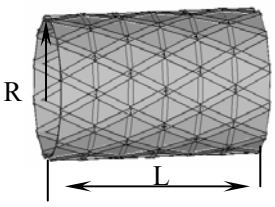

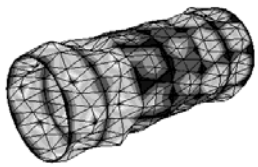

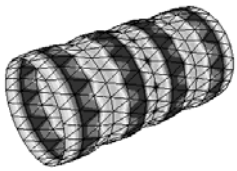

Fig.1 The AGS shell Fig.2 Eigen buckling mode Fig.3 Postbuckling mode

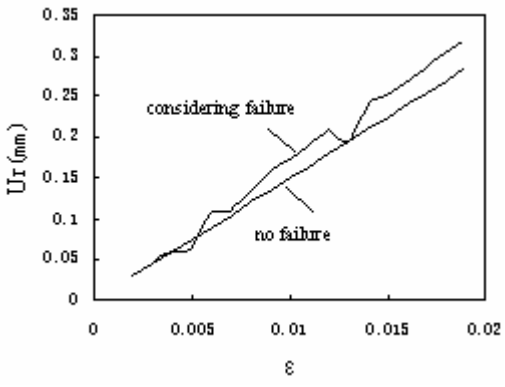

(a) Without considering thermal effect

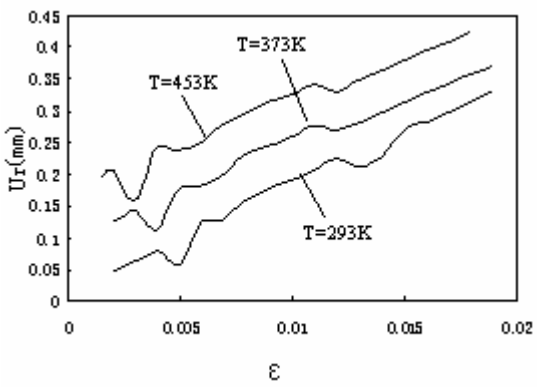

(b) Considering both the thermal effect and failure

Fig.4 The radial displacement vs. the axial compressive stain ε

For the three different cases namely without considering progressive failure, considering progressive failure and considering both the progressive failure and thermal effect, the radial displacement vs the axial compressive stain ε is shown in Fig.4. The point are selected for graphic presentation because it has the maximum radial displacement. From the curves in Fig.4(a), it can be seen that the skin of the AGS exhabits a highly local geometric nonliear behavior when considering the progressive failure. The stiffness of the damaged skin degraded remarkably. High temperature can cause a early failure, because the change of temperature will transform to thermal load applied on the strcture.

As the edge compressive axial stain ε reaches to 0.005, the matrix failure takes place in all layers to a certain extent. When ε reaches to 0.006, the zone containning matrix failure extends, and fiber-matrix shear failure occurs. As the edge-strain reach to 0.02, fiber failure occurs in the small area of the 1-4 and 17-20 layers. With further increase of the strain to 0.028, fiber failure occurs in the 5-8 and 13-16 layers at last.

Conclusions

The stiffness degradation caused by the progressive failure during the course of load-bearing prevent the AGS from achieving their theoretical elastic buckling strength. Thus, the post buckling analysis considering progressive failure and environment effects should generally be used in actual engineering analyses.

Acknowledgements

The authors are grateful to the support of National Natural Science Foundation in China, Grant No. 10302004.

References

[1] S. M. Huybrechts, T. E. Meink, P. M. Wegner, J. M.Ganley. Manufacturing Theory for Advanced Grid Stiffened Structures. Composites Part A: Applied Science and Manufacturing. 33, (2001), p.155.

[2] J. Higgins, P. Wegner, A. Viisoreanu, G.Sanford. Design and testing of the Minotaur advanced grid-stiffened fairing. Composite Structures, 66(2004), p.339.

[3] B.P. Patel, M. Ganapathi, D. P. Makhecha. Hygrothermal effects on the structural behaviour of thick composite laminates using higher-order theory. Composite Structures, 56(2002), p.25.

[4] Z.Sereir, E. Adda-Bedia, A.Tounsi. Effect of temperature on the hygrothermal behaviour of unidirectional laminated plates with asymmetrical environmental conditions. Composite Structures, 72(2006), p.383.

[5] R.Damodar, J. N. Ambur, M. Hilburger. Progressive failure analyses of compression-load composite curved panels with and without cutouts. Composite Structures, 65(2004), p.143.